Deformation mechanisms of stone column-improved liquefiable sloping ground under earthquake loadings

Yan-Guo Zhou*, Kai Liu

MOE Key Laboratory of Soft Soils and Geoenvironmental Engineering, Institute of Geotechnical Engineering, Zhejiang University, Hangzhou 310058, P. R. China
*E-mail: qzking@zju.edu.cn

Abstract. Liquefaction-induced deformation in sloping ground caused heavy damage to lifelines and overlaid structures in the past earthquake events. However, there is still a great need for estimation of large deformation of sloping ground during earthquakes and the associated deformation mitigation method. In this paper, a series of element tests were conducted to investigate residual volumetric strain and shear strain of soil element with initial shear stress, corresponding to infinite sloping ground condition. The element test results indicate that residual volumetric strain estimation method proposed by Shamoto and Zhang for level ground could be able to estimate that in sloping ground with initial static stress condition, and the residual shear strain is well correlated with maximum shear strain. In addition, a series of centrifuge model tests with respect to stone column improved sloping ground were designed and conducted to explore the effect of densification and drainage of stone column on deformation in sloping ground. The mechanisms of settlement and lateral spreading mitigation by densification and drainage effect of stone columns in sloping ground were analyzed and discussed in combination with centrifuge model tests and numerical simulation results. The present study provides an effective method for evaluating post-liquefaction settlement and deep insights of deformation mitigation of stone column in sloping ground, which is of great help for developing the performance-based mitigation method for sloping ground in the future.

Keywords: Post-liquefaction deformation, sloping ground, stone columns, centrifuge model test, numerical simulation.

1 Introduction

The past earthquakes have witnessed great damage to existing buildings and underground structures caused by liquefaction-induced lateral displacement in mildly sloping ground or nearly level ground with a free face (Bradley et al. 2019). Some studies have focused on this problem and several methods have been proposed to predict the lateral spreading in sloping ground (e.g., Youd et al. 2002; Zhang et al. 2004). In order to reduce the risk of liquefaction and associated ground deformation, stone column (SC) has been used in the past over forty years, and considerable in-situ cases have proved its effectiveness. Badanagki et al. (2018) conducted a series centrifuge model tests and found that greater area replacement ratios of SC (A_r) is effective to reduce the seismic settlement and lateral deformations in gentle slopes. Zhou et al.

(2021) performed three centrifuge models to individually investigate the effects of densification and drainage effect on level ground and concluded that the densification effect was the main factor and the drainage effect played the second role to reduce the settlement in a SC-improved ground. Besides, the three-dimensional numerical simulations conducted by Elgamal et al. (2009) and Asgari et al. (2013) showed that SC remediation was effective in reducing the sand stratum lateral deformation in sloping ground, the permeability of SC was a significant role in their cases.

In this paper, a series of element tests with initial shear stress using Hollow Cylinder Apparatus (HCA) were conducted to investigate the residual volumetric strain and shear strain. Besides, three centrifuge model tests were performed to explore the seismic performance of SC-improved sloping ground and worked as benchmarks to validate the constitutive model and numerical method. Based on both physical observations and numerical simulation results, the mechanisms of SC on deformation mitigation of sloping ground were preliminarily explored.

2 Post-liquefaction deformation with initial shear stress

2.1 S-Z method for post-liquefaction deformation in level ground

Shamoto and Zhang (1998) proposed a method for estimation of seismic settlement and horizontal displacement in level or nearly level ground (abbreviated as S-Z method in the following), based on constitutive analysis and element test evidence. According to their study, the residual volumetric strain (ε_{vr}) of a soil element could be expressed by,

$$\varepsilon_{v,r} = \frac{e_0 - e_{\min}}{1+e_0} R_0 \cdot \gamma_{\max}^m - M_{CS.0}\gamma_{0,r} - \frac{M_{CS} - M_0}{\alpha}\gamma_{d,r} \tag{1}$$

where e_0 and $e_{\min}$ are initial and minimum void ratio of soil, respectively; $\gamma_{\max}$, $\gamma_{0,r}$ and $\gamma_{d,r}$ are maximum shear strain, residual shear strain component independent of effective stress and residual shear strain component dependent on change in effective stress, respectively; M_{cs}, M_0 are slope of CSL (critical state line) and PTL (phase transformation line), respectively; $M_{cs.0}$ is the deviator-isotropic stress ratio at very small effective stress; R_0 and m are fitting parameters. Given that the undrained loading history is the same, ε_{vr} would reach its maximum value $(\varepsilon_{vr})_{\max}$ only when residual shear strain remains zero, namely,

$$\varepsilon_{v,r}\big|_{\gamma_r=0} = (\varepsilon_{v,r})_{\max} = \varepsilon_{vd,ir} = \frac{e_0 - e_{\min}}{1+e_0} R_0 \cdot \gamma_{\max}^m \tag{2}$$

2.2 The validity of S-Z method in sloping ground

In order to explore the effectiveness of above equations to sloping ground condition (i.e., initial shear stress condition), a series of undrained cyclic torsional shear tests (HCA) followed by reconsolidation were conducted, the ε_{vr} values were obtained to check the effectiveness of above expressions proposed by Shamoto and Zhang

(1998).The torsional shear tests were conducted by using hollow cylinder apparatus (HCA), which details could be referred to Chen et al. (2016). The testing material is Ottawa F-65 sand with 10% Qiantang river silt, the grain size distribution and physical properties are shown in Fig. 1 and Table. 1. The specimen has an outer diameter of 100 mm, an inner diameter of 60 mm, and a height of 200mm. The specimen was prepared by placing soils in eight layers in a traxial mold using the dry deposition method. The actual relative densities of all specimens after consolidation are about 60%. After the specimens were placed in the cell, the outer and inner pressures of 20 kPa were applied, then a two-stage saturation (carbon dioxide flushing and de-aired water flushing) was carried out to ensure the Skempton's B-value of 0.95 or larger. The effective stress is 100 kPa and two initial shear stress ratio (CSR_0)were designed, where $CSR_0=\tau_{ini}/\sigma'_c$ (σ'_c is average consolidation stress, τ_{ini} is initial shear stress).

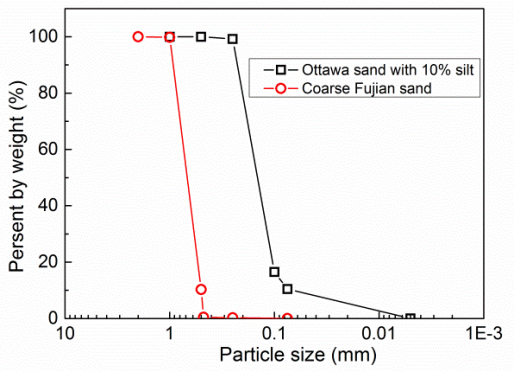

Fig. 1. Grain size distribution curves of two sands

Table 1. Physical properties of two sands.

Soil type	G_s	ρ_{max}(g/cm^3)	ρ_{min}(g/cm^3)	permeability (10^{-5} m/s)
Silty sand (Ottawa sand with 10% of silt)	2.673	1.921	1.510	2.7-5.6
Coarse Fujian sand	2.644	1.713	1.489	1490-3600

The specimens were isotropically consolidated by increasing the effective stress state up to 100 kPa, then the stress state was modified by applying a drained monotonic torsional shear stress up to a specified initial shear stress. Finally, undrained constant cyclic torsional loading was applied until the shear strain reached the expected value. Then the torsional shear stress was adjusted to the initial value under undrained condition followed by the reconsolidation process in constant shear stress ($\tau=\tau_{ini}$) with nearly constant γ_r.

For specimen without τ_{ini}, the specimens were isotropically consolidated followed by undrained constant cyclic torsional loading up to the expected shear strain, after that, the shear strain was adjusted to zero under undrained condition, and zero shear

strain state was kept in the drained reconsolidation process. The above procedure is consistent to that testing procedure of Shamoto and Zhang (1998) to eliminate the effect of γ_r on ε_{vr}.

Fig. 2 is a typical non-symmetrical stress-strain curve of a soil element with initial shear stress, where the maximum shear strain (γ_{max}) is usually defined as the strain increment from one stress reversal to the next. The γ_r is defined as the shear strain at shear stress (τ)=τ_{ini} for each cycle, which is consistent to Chiaro et al. (2012).

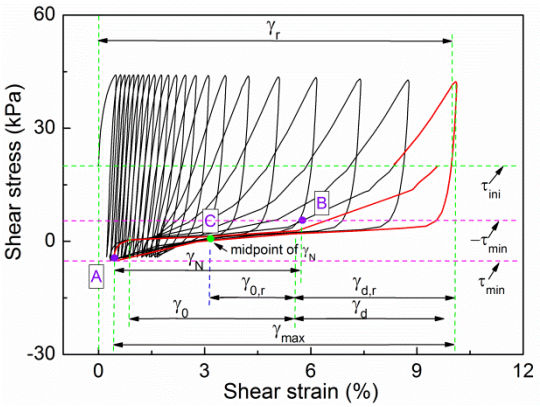

Fig. 2. Definition of shear strain components in non-symmetrical stress strain loop

Fig. 3(a) shows ε_{vr} versus γ_{max} for all element tests with and without initial shear stress. It is obvious that the ε_{vr} values for tests with CSR_0>0.0 are significantly smaller than that with CSR_0=0.0, it may attribute to that the existence of γ_r reduce the value of $(\varepsilon_{vr})_{max}$, as expressed by Eqs. (1) and (2). For CSR_0=0.0, ε_{vr} could reach its maximum value of $(\varepsilon_{vr})_{max}$, becauseγ_r remained zero during reconsolidation process. In order to confirm the validity of Eq. (1) for cases of CSR_0>0.0, the following attempts were made to obtain the parameters and residual shear strain components ($\gamma_{0,r}$ and $\gamma_{d,r}$). The parameters of M_{cs} and M_0 were determined by traxial element tests as 1.33 and 1.14 for this kind of silty sand, respectively. Following the suggestion of Shamoto and Zhang (1998), $M_{cs.0}$ was determined as $0.142M_{cs}$, and α was taken as $1.5\sqrt{3}$.For cases of CSR_0>0.0, $(\varepsilon_{vr})_{max}$ could be obtained by,

$$\varepsilon_{vd,ir} = (\varepsilon_{v,r})_{\max} = \varepsilon_{v,r} + M_{CS.0}\gamma_{0,r} + \frac{M_{CS} - M_0}{\alpha}\gamma_{d,r} \tag{3}$$

Another key issue is to determine the values of $\gamma_{0,r}$ and $\gamma_{d,r}$ in Eq. (3). It could be found in Fig. 2 that the residual shear strain started to accumulate toward to positive direction at the first cyclic loading under the effect of initial shear stress, and the stress-strain loop enlarged and moved toward positive direction with the increase of loading cycles. The movement of stress-strain loop reflects the change of element shape but not the irreversible volume strain accumulation. For this reason, the "base point" of the last stress-strain loop is depicted in Fig. 2 as point "C", it is the midpoint of shear strain increment from point "A" and "B", which are intersections of shear

stress τ=-τ_{ini} line and τ=τ_{ini} line and the last stress-strain loop, respectively, as shown in Fig. 2. The $\gamma_{0,r}$ and $\gamma_{d,r}$were determined following the suggestions of Shamoto and Zhang (1998). Fig. 3(b) clearly shows that the revised maximum residual volumetric strain for cases of CSR_0>0.0 are well consistent to that of CSR_0=0.0. The above result indicates that the settlement estimation method proposed by Shamoto and Zhang (1998) for level ground could be applied to sloping ground condition with the premise of accurate determination of residual shear strain components (i.e., $\gamma_{0,r}$ and $\gamma_{d,r}$).

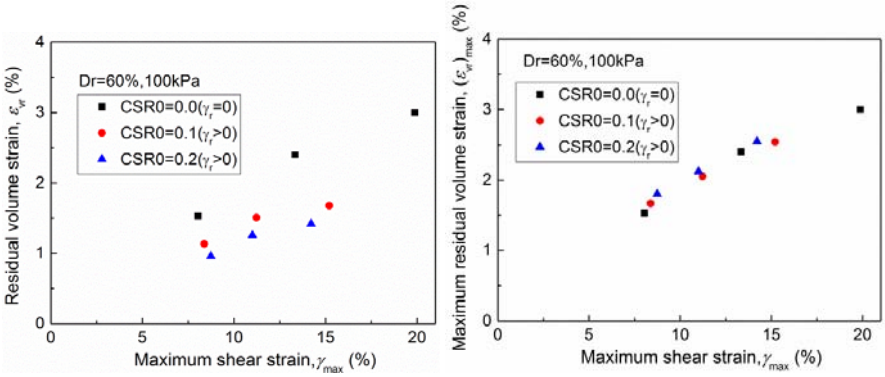

Fig. 3. The relation of maximum shear strain versus: (a) residual volumetric strain; (b) maximum residual volumetric strain

Residual shear strain has been paid more attention in the sloping ground for it closely relates to lateral spreading.. Fig. 2 illustrates how to determine the γ_r and γ_{max} in one cycle, and Fig. 4 shows the γ_r versus γ_{max} in this study. Also the data points for each CSR_0 are scattered, it is clearly found that the γ_r is positively correlated with γ_{max}. What's more, the γ_r value is obviously larger for larger value of CSR_0 under the same value of γ_{max}.

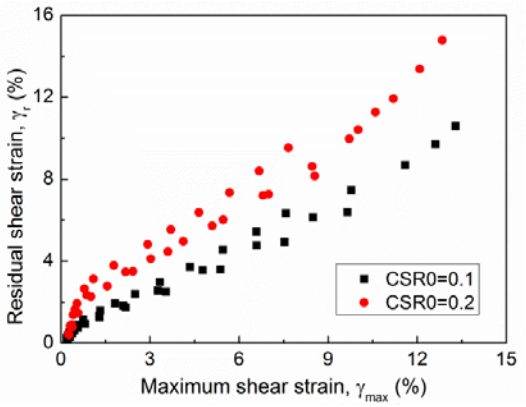

Fig. 4. The relation of maximum shear strain versus residual shear strain

3 Observations in centrifuge model tests

3.1 Test material and model configuration

A series of three centrifuge model tests were conducted to explore the effect of densification and drainage effect of stone column on seismic responses of sloping ground, following the same design conception from Zhou et al. (2021). Model 1 and Model 2 were designed to explore the densification effect only, both models do not include stone columns but are uniform silty sand ground. Model 1 is a loose pre-improved ground with initial void ratio of e_0, Model 2 represents the post-improved dense soil ground with void ratio of e_1. Model 2 and Model 3 were designed to explore the drainage effect of stone column, both models shared the same soil density, while stone columns were included in Model 3. The stiffness of stone column were designed to be close to that of surrounding soil to minimize the shear reinforcement.

The surrounding soil for three models was fine Ottawa F-65 sand with 10% of Qiantang river silt, and a coarse Fujian sand was chosen as stone column material. The grain size distribution curves are shown in Fig. 1 and physical properties for both materials are given in Table 1. Silicone oil with viscosity 50 times that of water was used as pore fluidt.

The side and top views of model configuration of Model 3 are shown in Fig. 5, the model configuration for Model 1 and Model 2 are almost the same but both models were uniform silty sand ground. Accelerometers pore pressure transducers were placed in the center of the model ground, three pairs of bender elements were also installed. . Two LVDT transducers were installed to record the surface settlement of the model ground.

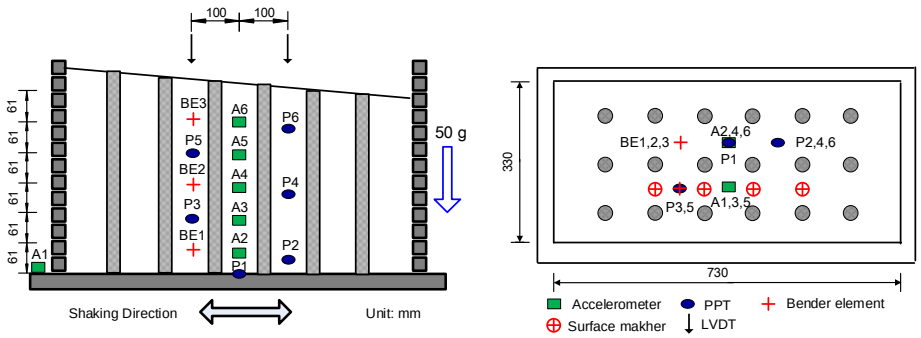

Fig. 5. Model configuration (geometry in model scale) of Model 3

3.2 Model preparation and test procedure

The fine Ottawa sand and Qiantang river silt were fully mixed with a mass ratio of 9:1. Model 1 was prepared using air pluviation method with relative density(D_r) =50%. Model 2 and Model 3 were prepared using dry tamping method with D_r=78%.

The diameter-to-spacing (d/s) parameter in Model 3 was determined following Zhou et al. (2017) as 0.3, the diameter and spacing for SCs are 3 cm and 10 cm in model scale, and the area replacement ratio (A_r) $=\pi d^2/(4s^2)=7\%$. The SC installation method is the same as that adopted by Zhou et al. (2021). All three models were saturated by vacuum method.

The centrifuge tests were conducted under 50 g, shear wave velocities at different depths of the model ground were measured by bender elements and then the destructive sine wave motion followed. Long enough time interval was waited for the full dissipation of excess pore water pressure (EPWP) induced by previous shaking in the model ground.

The designed shaking sequences of three models are the same, as shown in Fig. 6, to compare the differences of seismic response among three models. The input motion was a sine wave of fifteen constant cycles with dominant frequency of 1 Hz.

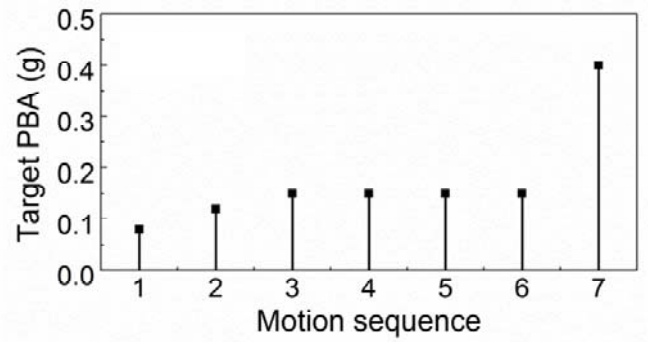

Fig. 6. Target shaking sequence in three model tests

3.3 Experimental results and analysis

The dynamic responses among three models were compared and analyzed to distinguish the effect of individual densification and drainage on seismic responses in sloping ground. Fig. 7 shows the seismic responses between Model 1 and 2 under motion1. It could be found that densification in Model 2 slowed down the generation rate and lowered the peak of EPWP ratio at all depth. The acceleration at shallow depth in Model 1 (ie., depth=0.5 m and 3.5 m) were de-amplified only in upslope direction but significantly amplified by high-frequency negative spikes in downslope direction. This phenomenon is only observed at shallow depth in Model 2 due to soil disturbance during modeling, the acceleration at other depths were similar to the input base motion.

Fig. 7(c) depicts the stress-strain loops of Model 1 and Model 2, it is obvious that densification of Model 2 reduced the shear strain at shallow depth (i.e., 3.5 m and 6.5 m), which could be attributed to the increase of shear stiffness after densification.

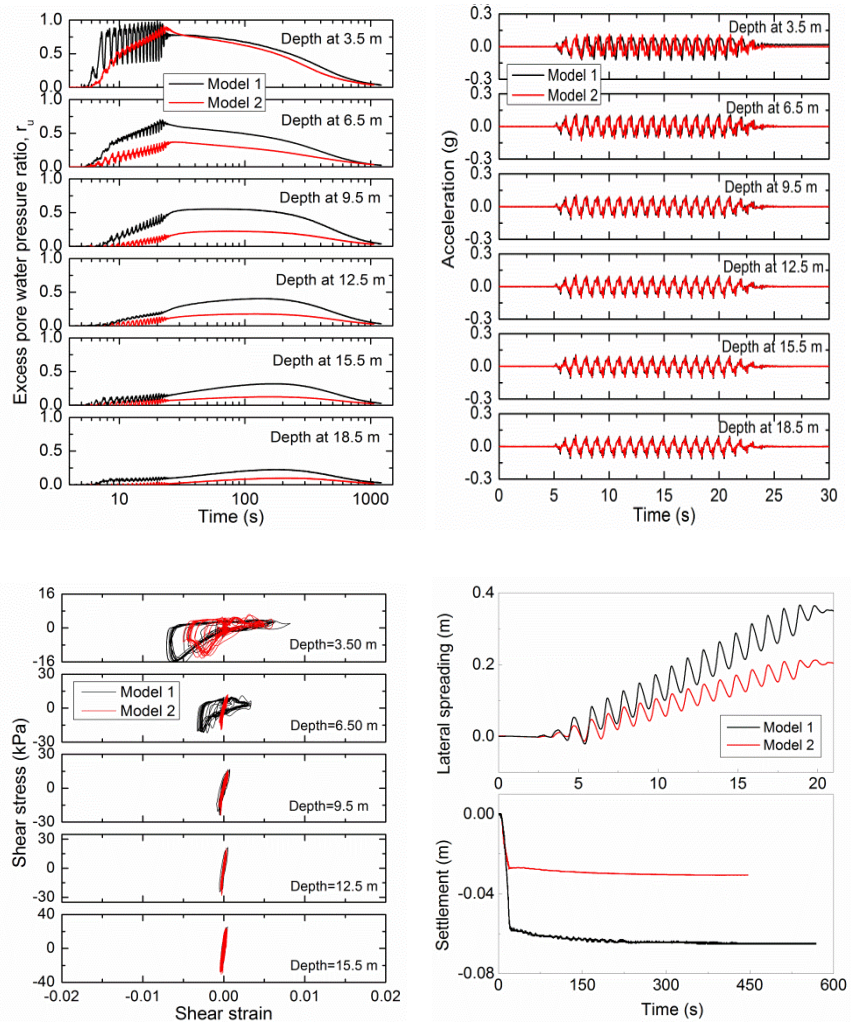

Fig. 7. Seismic responses of Model 1 and Model 2 under motion 1

Fig. 8 compares the seismic responses between Model 2 and Model 3 under motion3. It is found that peaks of EPWP at most depth were quite comparable between two models, while the EPWP generation rate during shaking was significantly slower at shallow depth in Model 3 due to the drainage effect. In addition, the time for fully dissipation of EPWP in Model 3 was shortened at all depth. The acceleration responses at shallow depth (i.e., depth at 3.5 m) showed significant positive spikes in Model 3 compared to that of Model 2, and the acceleration at other depths were nearly the same between two models.

Fig. 8(c) shows the stress-strain curves for Model 2 and Model 3. It is found that shear strain at all depth (i.e., depth above 6.5 m) were compatible between two model. The cyclic mobility phenomenon was only observed in downslope direction in Model

2 at shallow depth, while they were obvious in both downslope and upslope directions in Model 3.

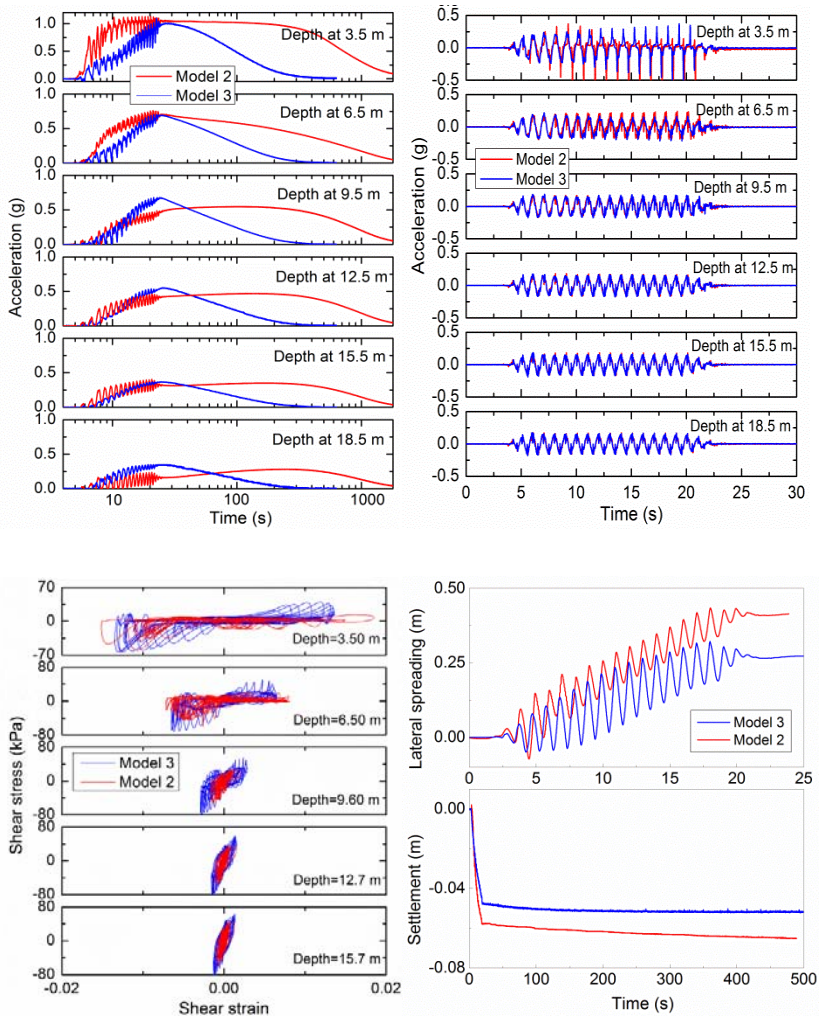

Fig. 8. Seismic responses of Model 2 and Model 3 under motion 1

4 Findings from numerical simulation

4.1 Calibration of constitutive model parameters

The unified plasticity model (CycliqCPSP), proposed by Wang et al. (2014), was adopted here to simulate stone column and silty sand materials, because it could properly reflect the dilatancy of sand and larger shear deformation under cyclic loading.

This model introduces the state parameter concept thus enabling it to model sand under different states with the same set of parameters, and it has been implemented into finite differencecode FLAC3D. It incorporates 14 parameters listed in Table 3, including elastic modulus constants (G_0, κ), plastic modulus parameter (h), critical state parameters (M, λ_c, e_0, ξ),state parameter constants (n_p, n_d), dilatancy parameters ($dre_{,1}$,$dre_{,2}$, dir, α, $\gamma_{d,r}$). The model parameters were determined followingthe methods suggested by Wang et al.(2014) and He et al. (2020).

A set of high-fidelity hollow cylinder torsional shear tests and traxial tests were conducted as benchmark element tests to calibrate the silty sand and stone column materials, respectively. The physical properties of two sands are as shown in Table 1. The model parameters are adopted as listed in Table 3, and the comparisons between tests and simulations in Fig. 9 show good agreement, especially for the post-liquefaction shear deformation.

Table 3. Model parameters for CycLiqCPSP model used in the numerical simulations.

Parameters	G_0	κ	h	M	λc	e_0	ξ
Sility sand	234	0.01	1.6	1.19	0.022	0.715	0.71
Stone column	353	0.01	1.2	1.28	0.029	0.788	0.70
Parameters	n_p	n_d	$dre_{,1}$	$dre_{,2}$	dir	α	$\gamma_{d,r}$
Sility sand	3.4	5.3	1.1	30	1.35	5.0	0.05
Stone column	1.4	8.0	1.1	30	1.10	30	0.05

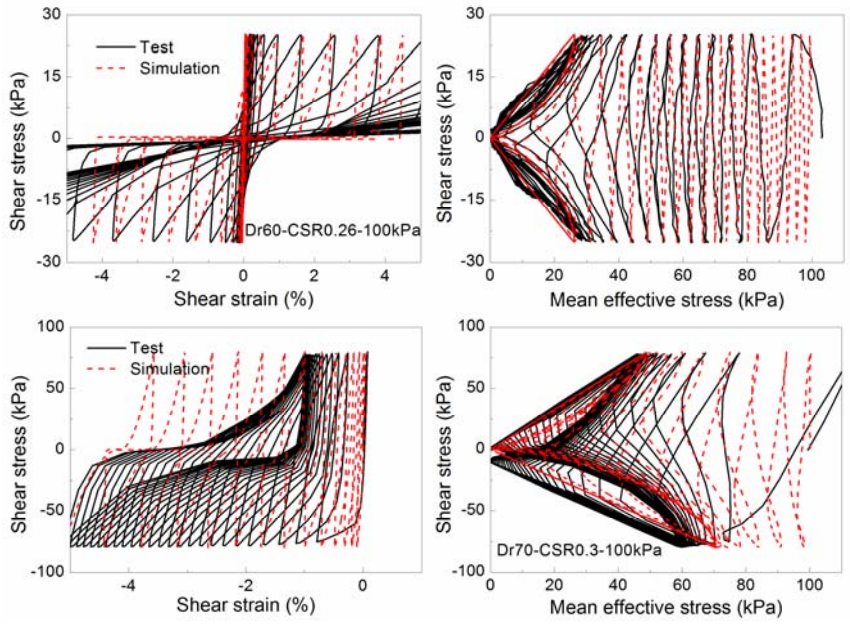

Fig. 9. Comparison between model tests and simulations: (a) Silty sand; (b) stone column

4.2 Numerical model configuration

A shown in Fig. 10, the plane strain numerical model was used for Model 1 and Model 2. The numerical model was constructed in prototype dimensions under 1g gravity field. Fully coupled effective stress analysis was conducted. The initial stress state of the model was obtained using rigid box condition, then the displacement degrees of freedom for soil nodes at lateral boundaries along the shaking direction are set free, and the laminar box condition was configured to re-calculate the initial stress state. Two one-dimension columns were configured to reflect the laminar box, the nodes of which at the same elevation are tied to each other and elastic model were adopted with Young Modulus (E)=3e5 kPa, poison ratio=0.32. As for dynamic stage, the processed acceleration record was applied at base nodes and long enough time is needed for fully dissipation of excess pore water pressure. Small Rayleigh damping of 1% is assigned for numerical stability and to control high frequency numerical noise.

A 3D numerical model was established for Model 3 to properly reflect the 3D condition of stone column-improved ground, it has the same dimensions as the model test in prototype scale and consists of 31900 meshes for soil materials (As shown in Fig. 10). The cylinder gravel drains are simulated with equivalent squares of the same cross section area. The permeability coefficient of the two sands are adopted the real values in Table 1. As for 3D numerical model, the displacement degree of freedom for soil nodes are free perpendicular to the shaking direction, and only soil nodes at the lateral boundary perpendicular to the direction are fix in y-direction. Other boundary conditions during static consolidation are consistent with those in 2D numerical model. The one dimensional columns in 2D model are replaced by two independent plates with one zone width to reflect the laminar box condition. The parameters of *E* for elastic model is adjusted as 5e4 kPa, and other parameters are the same as that in 2D model. Similarly, the nodes at two plates with the same elevation are tied each. Interface element is also used in 3D numerical simulation.

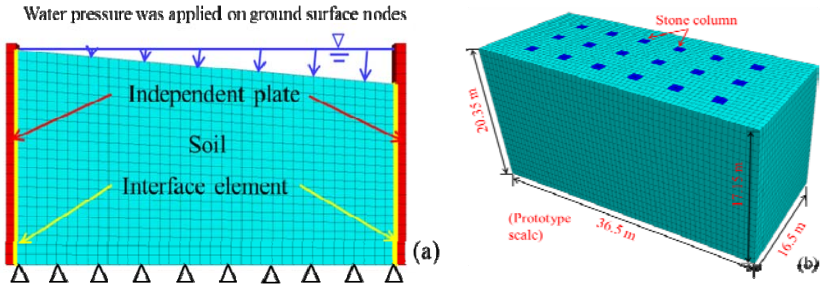

Fig. 10. Numerical model: (a)Side view of boundary condition during dynamic stage; (b) 3D model mesh for Model 3

Most available constitutive models would underestimate the settlement compared to what occurs in real condition (Shahir et al. 2014). The developers of CycliqCPSP introduced a settlement improved subroutine in FLAC3D to increase the accuracy of simulated settlement, which further reduce the soil modulus with respect to the cur-

rent effective stress and maximum shear strain level to simply increase post-shaking settlement. This subroutine could be switched on after shaking to significantly increase the accuracy of simulated post-shaking settlement. This subroutine was used here and the parameters were adopted as: C_{s_min}=0.2, C_1=0.02, C_2=0.0 and C_5=5.0.

4.3 Numerical simulation results

Figs. 11 and 12 compared the simulation and test results for Model 2 and Model 3 under motion1. The simulated acceleration and EPWP reasonably match with those of model tests, especially for the generation and dissipation of EPWP. The lateral displacement time histories of model test were obtained following the method proposed by Kutter et al. (2015). The residual lateral displacement and displacement development process are well simulated with the average surface lateral spreading of model tests, but the simulated displacement fluctuation tends to be smaller during shaking period. The simulated surface settlements also match well with those of test when the settlement improved subroutinewas adopted. The comparisons between simulation and model test for other motions were also consistent. The above results validate the effectiveness of CycliqCPSP and the used numerical method, which paves the way for further analysis on displacement characteristics of stone column improved ground in the future.

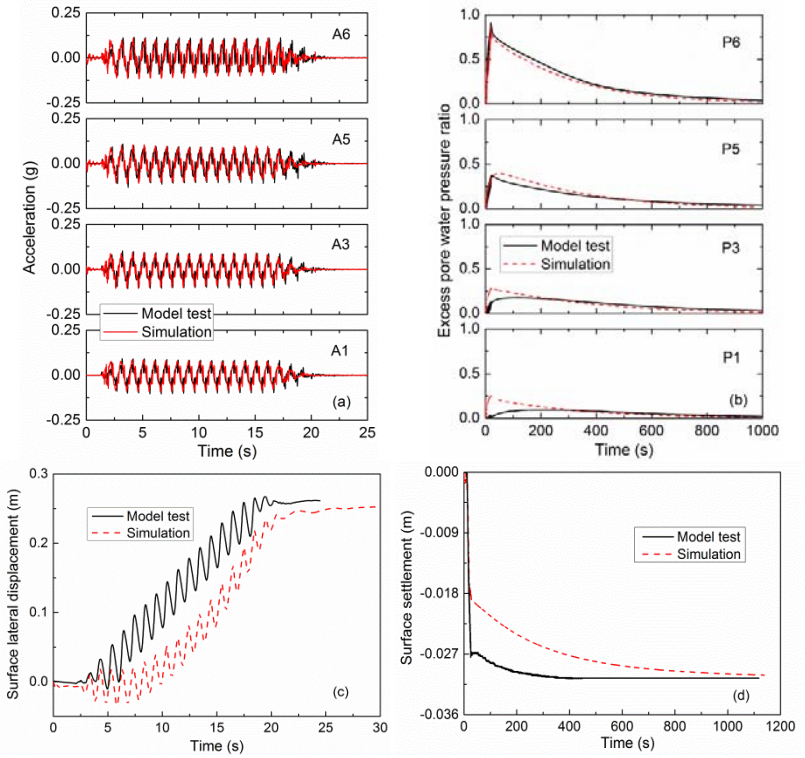

Fig. 11. Simulation and model test for Model 2 under motion1: (a) Acceleration time history; (b) Excess pore water pressure; (c) Average surface lateral spreading; (d) Surface settlement

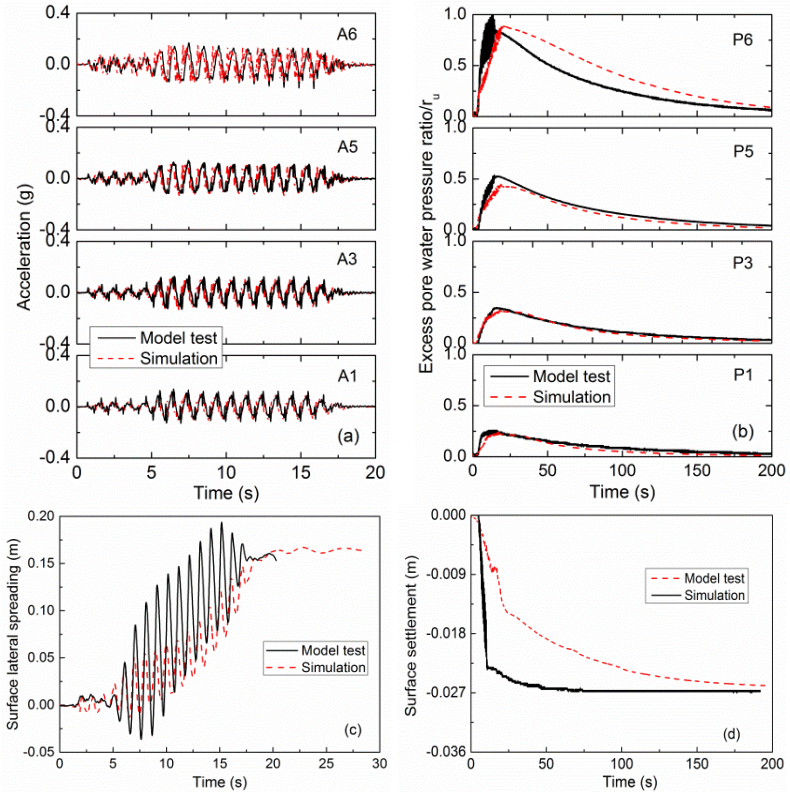

Fig. 12. Simulation and model test for Model 3 under motion1: (a) Acceleration time history; (b) Excess pore water pressure; (c) Average surface lateral spreading; (d) Surface settlement

5 Deformation mechanisms of stone column improved sloping ground

The above model tests and numerical simulation show that the densification and drainage effects of stone column could reduce both surface settlement and lateral spreading in sloping ground. However, the deformation mitigation mechanisms have not been well understood, which will be preliminarily discussed in the following section.

5.1 The effect of densification on settlement and lateral spreading

Dashti et al. (2012) identified several volumetric-induced settlement mechanisms as follows: 1) Localized volumetric strains during partially drained cyclic loading controlled by 3D transient hydraulic gradients ($\varepsilon_{\text{p-DR}}$); 2) Settlements due to sedimenta-

tion or solidification after liquefaction or soil structure break-down ($\varepsilon_{p\text{-}SED}$) and; 3) Consolidation-induced volumetric strains as excess pore pressures dissipate ($\varepsilon_{p\text{-}CON}$).

The soil skeleton after densification would become more intact with less void ratio, it will undergo less extent of soil skeleton breakdown under the same input energy, which helps to reduce the sedimentation-induced settlement.

Consolidation-induced settlement is essentially the process of soil's compression under soil own-weight over time, so it is mainly influenced by the compressibility of soil, which is conventionally expressed by compressive modulus. It is well-known compressive modulus is mainly influenced by effective stress level, it comes close to zero when soil is liquefied. In this sense, densification could significantly reduce the EPWP level (as shown in Fig. 7), thus reducing the softening extent of soil under the same shaking input motion, resulting in a less consolidation-induced settlement.

Fig. 4 has validated the relation between residual shear strain and maximum shear strain. It is well understood that the shear modulus of soil will increase after densification, which will reduce the shear strain when soil undergoes the same shaking intensity, as shown in Fig. 7, so densification could reduce the residual shear strain in sloping ground. Fig. 7 also shows that the soil will dilate to recover its shear modulus under smaller shear strain, which is of great help to reduce lateral spreading in sloping ground.

5.2 The effect of drainage on settlement and lateral spreading

It could be seen from Fig. 9 that drainage effect significantly slowed down the generation rate of EPWP during shaking and delayed the time of liquefaction occurring, which would reduce the extent of soil skeleton breakdown, thus reducing the contribution of sedimentation-induced settlement ($\varepsilon_{p\text{-}SED}$) to total settlement. Besides, drainage effect expedited the dissipation of EPWP after shaking and accelerated the recovery of compressive modulus of soil, which would reduce the consolidation-induced settlement ($\varepsilon_{p\text{-}CON}$). However, the drainage effect would increase the contribution of$\varepsilon_{p\text{-}DR}$ during cyclic loading to total settlement. In this paper, the reduction of $\varepsilon_{p\text{-}SED}$ and $\varepsilon_{p\text{-}CON}$ overcame the increase of $\varepsilon_{p\text{-}DR}$, resulting in the reduction of total settlement.

Fig. 8 shows that the maximum shear strain of Model 3 was smaller than that of Model 2 at shallow depth (i.e., depth=3.5 and 6.5 m), which is attributed to drainage effect. The reduction of maximum shear strain in Model 3would result in a smaller residual shear strain according to Fig. 4. The smaller shear strain in Model 3 could be attributed to that the drainage effect reduced the extent of water absorption of soil during shear, according to Zhang et al. (1999).

In addition, the stone column material has larger permeability coefficient and liquefaction resistance compared to that surrounding soil, the "stiffer" SCs underwent smaller lateral displacement thus restricting the lateral displacement of the surrounding soil, this phenomenon was well observed in numerical simulation, as shown in Fig. 13.

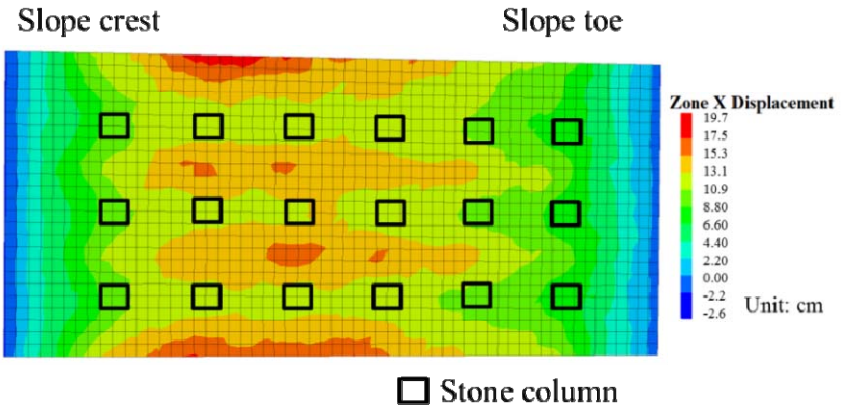

Fig. 13. Top view of surface lateral spreading of Model 3 under motion1

6 Conclusions

A series of HCA soil element tests were conducted to identify the residual volumetric and shear strain with initial stress condition, and three centrifuge model tests and numerical simulations were performed to explore the deformation mitigation mechanisms of stone column-improved sloping ground. Some interesting conclusions are drawn as follows:

(1) The settlement estimation method proposed by Shamoto and Zhang (1998) for level ground could be applied to sloping ground condition given the residual shear strain component, and the maximum dynamic shear strain were found to be well correlated with residual strain;

(2) The adopted constitutive model and numerical method were validated by the centrifuge model tests with respect to acceleration, EPWP and deformation response;

(3) The densification effect could reduce sedimentation and consolidation settlement by reducing soil skeleton breakdown and softening extent of soil under the same shaking intensity respectively, in addition, it reducing the maximum shear strain thus reducing the residual shear strain in sloping condition;

(4) The drainage effect slows down the generation rate of EPWP thus reducing the sedimentation settlement and reduces consolidation settlement by expedite the dissipation process of EPWP, besides, the “stiffer column” will restrict the lateral spreading of surrounding soil.

Acknowledgements

The authors would like to acknowledge the National Natural Science Foundation of China (Nos. 51988101, 51978613 and 51778573) and the Chinese Program of Introducing Talents of Discipline to University (the 111 Project, No. B18047) for the fund-

ing support. Sincere thanks to Prof. Guoxing Chen and Dr. Qi Wu of Nanjing Tech University for their help during the soil element test, and to Mr. Qiang Ma and Mr. Zizhuang Yan of Zhejiang University for their supports in conducting the centrifuge model tests.

References

1. Asgari, A., Oliaei, M., Bagheri, M.: Numerical simulation of improvement of a liquefiable soil layer using stone column and pile-pinning techniques. Soil Dynam. Earthq. Eng., 51:77-96 (2013).
2. Badanagki, M., Dashti, S., Kirkwood, P.: Influence of dense granular columns on theperformance of level and gently sloping liquefiable sites. J Geotech. Geoenviron.Eng., 144(9):04018065 (2018).
3. Chiaro, G., Koseki, J., Sato, T.: Effects of initial static shear on liquefaction and large deformation properties of loose saturated Toyoura sand in undrained cyclic torsional shear tests. Soils and foundations. 52(3): 498-510 (2012).
4. Elgamal, A., Lu, J., Forcellini, D.: Mitigation of liquefaction induced lateraldeformation in a sloping stratum: Three-dimensional numerical simulation. J Geotech. Geoenviron. Eng., 135(11):1672-82 (2009).
5. Wang, R., Zhang, J.M., Wang, G.: A unified plasticity model for large post-liquefactionshear deformation of sand. Comput. Geotech. 59, 54–66 (2014).
6. Shahir, H., Mohammadi-Haji B., Ghassemi A.: Employing a variable permeability model in numerical simulation of saturated sand behavior under earthquake loading. Computers and Geotechnics, 55:211-223(2014).
7. Shamoto,Y., Zhang, J.M., Tokimatsu, K.: New chartsfor predicting large residual post-liquefaction grounddeformation. Soil Dynam. Earthq. Eng. 17(7): 427–438 (1998).
8. Youd, T.L., Hansen, C.M., Bartlett, S.F.: Revisedmultilinear regression equations for prediction of lateralspread displacement. J Geotech. Geoenviron. Eng. 128(12): 1007–1017 (2002).
9. Zhang, G., Robertson, P.K., Brachman, R.W.I.: Estimating liquefaction-induced lateral displacements using the standard penetration test or cone penetration test. J Geotech. Geoenviron. Eng. 130(8): 861–871 (2004).
10. Zhang, J.M., Tokimatsu K., Taya Y.: Effect of water absorption in shear of post-liquefaction. Chinese Journal of Geotechnical Engineering, 21(4):398-404 (1999). (in Chinese).
11. Zhou, Y.G., Liu, K., Sun. Z.B., Chen Y.M.: Liquefaction mitigation mechanisms of stone column-improved ground by dynamic centrifuge model tests. Soil Dynam. Earthq. Eng. 106660 (2021).
12. Zhou, Y.G., Sun, Z.B., Chen, J., Chen, Y.M., Chen, R.P.: Shear wave velocity-basedevaluation and design of stone column improved ground for liquefactionmitigation. EarthqEngEngVib. 16(2):247–61 (2017).
13. Zou, Y.X., Zhang, J.M., Wang, G.: Seismic analysis of stone column improved liquefiable ground using a plasticity model for coarse-grained soil. Computers and Geotechnics. 125 (2020).
14. Bradley K, Mallick R, Andikagumi H, Hubbard J, Meilianda E, Switzer A, Du NR, Brocard G, Alfian D, Benazir B, Feng GC, Yun SH, Majewski J, Wei SJ, Hill EM. Earthquake-triggered 2018 Palu Valley landslides enabled by wet rice cultivation. Nat. Geosci. 2019; 12(11): 935-939.